

**POLYNOMIAL MODEL OF TRANSMISSION AND
REFLECTION OF ELECTROMAGNETIC WAVES
IN MULTILAYER THIN FILMS SUBJECTED TO
AN EXTERNAL TRANSVERSE VOLTAGE**

MOHAMMED K. M. ELHABBASH

UNIVERSITI SAINS MALAYSIA

2024

**POLYNOMIAL MODEL OF TRANSMISSION
AND REFLECTION OF ELECTROMAGNETIC
WAVES IN MULTILAYER THIN FILMS
SUBJECTED TO AN EXTERNAL TRANSVERSE
VOLTAGE**

by

MOHAMMED K. M. ELHABBASH

**Thesis submitted in fulfilment of the requirements
for the degree of
Doctor of Philosophy**

July 2024

ACKNOWLEDGEMENT

I am grateful for the support and guidance provided by my thesis advisors, Dr Mohd Mahadi Halim and Associate Professor Dr Tiem Leong Yoon. Their invaluable comments and feedback have guided me towards the successful completion of my thesis, while their expertise, patience, and dedication have played an instrumental role in shaping my research work and academic career. I am truly grateful for their mentorship, insightful feedback, and unwavering belief in my abilities. Thank you for your invaluable contribution to my success. I would also like to express my sincere gratitude to Professor Sofyan Taya for his unwavering support and encouragement throughout my academic journey. His expert advice and mentorship have played a crucial role in shaping my research interests and expanding my knowledge in the field. I would like to extend my heartfelt thanks to the dean, Prof. Dr Abdul Razak Ibrahim and all the members and staff at the school of physics, Universiti Sains Malaysia for their continuous support and encouragement throughout my academic journey. Their unwavering dedication to teaching and research has inspired me to strive for excellence in all my endeavours. Last but not least, to Prof. Dr Azlan Abdul Aziz, the dean of the Institute Postgraduate Studies (IPS) and the team members for taking input, advice and involvement in updating the USM Guidelines in finishing the template. A special dedication to the participants that had attended Research Support Workshop in USM Library. Thank you for the tremendous positive feedback given along with the continuous support received.

TABLE OF CONTENTS

ACKNOWLEDGEMENT	ii
TABLE OF CONTENTS.....	iii
LIST OF TABLES	v
LIST OF FIGURES	vi
LIST OF ABBREVIATIONS	xvi
LIST OF SYMBOLS	xvii
LIST OF APPENDICES	xix
ABSTRAK	xx
ABSTRACT	xxii
CHAPTER 1 INTRODUCTION.....	1
1.1 Motivation	1
1.2 Research Gap.....	1
1.3 Problem statement	2
1.4 Objectives	3
1.5 The scope and limitations of work	3
1.6 Contribution of the dissertation.....	4
1.7 Thesis outline and organization.....	4
CHAPTER 2 LITERATURE REVIEW.....	9
2.1 Modelling of EM interactions with a multilayer structure	11
2.2 Transfer matrix	12
2.3 ABCD matrix	14
2.4 Propagator matrix	16
2.5 Bi Characteristic Impedance Transmission Line and Conjugate Characteristic Impedance Transmission Line	19

CHAPTER 3	THEORY.....	23
3.1	Modelling of EM interactions with a multilayer structure using the polynomial method.....	23
3.2	Fresnel's coefficients of polarized EM waves for transverse magnetic mode (P-polarized) in a lossy, nonmagnetic medium.....	34
3.3	Fresnel's coefficients of polarized EM waves for transverse electric mode (S-polarized) in a lossy, nonmagnetic medium.....	46
3.4	Fresnel's coefficients of polarized EM waves for transverse magnetic mode (P-polarized) in a lossless, nonmagnetic medium.....	51
3.5	Fresnel's coefficients of polarized EM waves for transverse electric mode (S-polarized) in a lossless, nonmagnetic medium.....	52
3.6	Reflection, transmission, and their corresponding phases of a multilayer medium.....	53
CHAPTER 4	METHODOLOGY.....	56
4.1	The data collection	56
4.2	Implementation of the boundary conditions.....	56
4.3	Code verification	62
CHAPTER 5	RESULTS AND DISCUSSION.....	80
5.1	Results for lossy multilayer thin film of germanium/magnesium oxide (Ge/MgO).....	80
5.2	Results for lossless multilayer thin film of magnesium oxide/calcium fluoride (MgO/CaF ₂).....	95
5.3	Results for lossless multilayer thin film of magnesium oxide/calcium fluoride (CaF ₂ /SiO ₂).....	107
CHAPTER 6	CONCLUSIONS	113
REFERENCES.....		118
APPENDICES		
LIST OF PUBLICATIONS		

LIST OF TABLES

	Page
Table 2.1 A ray transfer matrix for basic optical elements.	16
Table 4.1 The values of optical parameters of one-layer thin film of Ge, MgO, CaF ₂ , and SiO ₂ with their corresponding calculated Brewster angles, transmission and reflection Fresnel's coefficients at a condition of Brewster angles for each material.....	60
Table 4.2 The values of optical parameters of one-layer thin film of Ge, MgO, CaF ₂ , and SiO ₂ with the corresponding calculated critical angles.....	61
Table 4.3 The values of parameters used in the Wave Tensor and Wave Tensor-II code for Ge, MgO, CaF ₂ , and SiO ₂ thin films along with the corresponding Brewster angles, extracted from Figure 4.4, Figure 4.5, Figure 4.6, and Figure 4.7.....	68
Table 4.4 The Fresnel's coefficients along with the corresponding Brewster angles for 1-layer Ge, MgO, CaF ₂ , and SiO ₂ extracted from Figure 4.4, Figure 4.5, Figure 4.6, and Figure 4.7 synthesized by the Wave Tensor (WT) and (WT-II) code.....	69
Table 4.5 The values of parameters used in the Wave Tensor and Wave Tensor-II code for Ge, MgO, CaF ₂ , and SiO ₂ thin films along with the corresponding critical angles, extracted from Figure 4.8, Figure 4.9, Figure 4.10, and Figure 4.11.	74

LIST OF FIGURES

	Page
Figure 2.1	Propagation of a plane electromagnetic wave through a multilayer thin film consists of N layers. Propagation of the electric field is from the left boundary at $z = z_1$ to the right boundary at $z = z_{N+1}$... 13
Figure 2.2	Definition of the transverse offset and offset angle before and after the optical system. 15
Figure 2.3	The model employed for a lossy transmission line with multiple sections, known as the bi-characteristic impedance transmission line (BCITL) model. 20
Figure 3.1	A thin film consisting of N layers, each layer and the interface between them labelled by the index j . The thickness of the j th interface is denoted by δz_j , while the angles of incidence and propagation are indicated as $\theta_0, \theta_1, \dots, \theta_N$. The electromagnetic wave is assumed to propagate in the positive z -direction, from left to right. 30
Figure 3.2	A setup shows how waves reflect ('r') and transmit through('t') at the border between two semi-infinite dielectric slabs, when hit by a wave incident from the left ('i'), for a TM wave. In this case, the electric field moves only in the x and z directions, and the magnetic field travels solely in the y -direction. 38
Figure 3.3	Configuration of the reflected and refracted waves at an interface between two adjacent dielectric semi-infinite slabs for the TE mode. Note that in TE mode, the magnetic field has components in the x - and z -directions, while the electric field has only a component in the y -direction. 47
Figure 4.1	The 1-layer thin film. 58
Figure 4.2	Pseudocode of the Wave Tensor code 65
Figure 4.3	Flowchart of the Wave Tensor code. 67

- Figure 4.4 Plots of a: r^α vs. θ_0 , b: $(r^\alpha)^2$ vs. θ_0 , c: t^α vs. θ_0 and d: $(t^\alpha)^2$ vs. θ_0 for $\alpha \in TE, TM$ produced by the WT-II code for Ge at $\lambda_0 = 540$ nm. The vertical line marks the theoretical value of $\theta_B = 75.861^\circ$. Note specifically that the vertical line coincides with the zero of r^{TM} and $(r^{TM})^2$ 70
- Figure 4.5 Plots of a: r^α vs. θ_0 , b: $(r^\alpha)^2$ vs. θ_0 , c: t^α vs. θ_0 and d: $(t^\alpha)^2$ vs. θ_0 for $\alpha \in TE, TM$ produced by the WT code for MgO at $\lambda_0 = 542$ nm. The vertical line marks the theoretical value of $\theta_B = 60.13^\circ$. Note specifically that the vertical line coincides with the zero of r^{TM} and $(r^{TM})^2$ 71
- Figure 4.6 Plots of a: r^α vs. θ_0 , b: $(r^\alpha)^2$ vs. θ_0 , c: t^α vs. θ_0 and d: $(t^\alpha)^2$ vs. θ_0 for $\alpha \in \{TE, TM\}$ produced by the WT code for CaF₂ at $\lambda_0 = 542$ nm. The vertical line marks the theoretical value of $\theta_B = 55.13^\circ$. Note specifically that the vertical line coincides with the zero of r^{TM} and $(r^{TM})^2$ 72
- Figure 4.7 Plots of a: r^α vs. θ_0 , b: $(r^\alpha)^2$ vs. θ_0 , c: t^α vs. θ_0 and d: $(t^\alpha)^2$ vs. θ_0 for $\alpha \in \{TE, TM\}$ produced by the WT code for SiO₂ at $\lambda_0 = 2500$ nm. The vertical line marks the theoretical value of $\theta_B = 55.0312^\circ$. Note specifically that the vertical line coincides with the zero of r^{TM} and $(r^{TM})^2$ 73
- Figure 4.8 Plots of a: r^α vs. θ_0 , b: $(r^\alpha)^2$ vs. θ_0 , c: t^α vs. θ_0 and d: $(t^\alpha)^2$ vs. θ_1 for a polarized EM wave with an initial wavelength of 5.4 μm propagates from one-layer Ge thin film to vacuum. The vertical

line marks the theoretical value of critical angle, $\theta_c = 14.5898^\circ$, which are seen to coincide with the values $r^{TM} = -1$, and $r^{TE} = 1$ on the curves produced by the Wave Tensor code.....75

Figure 4.9 Plots of a: r^α vs. θ_0 , b: $(r^\alpha)^2$ vs. θ_0 , c: t^α vs. θ_0 and d: $(t^\alpha)^2$ vs. θ_1 for a polarized EM wave with an initial wavelength of 542 nm propagates from one-layer MgO thin film to vacuum. The vertical line marks the theoretical value of critical angle, $\theta_c = 35.04^\circ$, which are seen to coincide with the values $r^{TM} = -1$, and $r^{TE} = 1$ on the curves produced by the Wave Tensor code.....76

Figure 4.10 Plots of a: r^α vs. θ_0 , b: $(r^\alpha)^2$ vs. θ_0 , c: t^α vs. θ_0 and d: $(t^\alpha)^2$ vs. θ_1 for a polarized EM wave with an initial wavelength of 542 nm propagates from one-layer CaF₂ thin film to vacuum. The vertical line marks the theoretical value of critical angle, $\theta_c = 44.17^\circ$, which are seen to coincide with the values $r^{TM} = -1$, and $r^{TE} = 1$ on the curves produced by the Wave Tensor code.....77

Figure 4.11 Plots of a: r^α vs. θ_0 , b: $(r^\alpha)^2$ vs. θ_0 , c: t^α vs. θ_0 and d: $(t^\alpha)^2$ vs. θ_1 for a polarized EM wave with an initial wavelength of 542 nm propagates from one-layer SiO₂ thin film to vacuum. The vertical line marks the theoretical value of critical angle, $\theta_c = 44.3787^\circ$, which are seen to coincide with the values $r^{TM} = -1$, and $r^{TE} = 1$ on the curves produced by the Wave Tensor code.78

Figure 5.1 The curves $R(\lambda)$, $\phi_R(\lambda)$, $T(\lambda)$, and $\phi_T(\lambda)$ for a non-obliquely incident electromagnetic wave, $\theta_0 = 0^\circ$. These curves have been synthesized using the WT-II code for a germanium (Ge) 1-layer film without implementing any transverse electrical potential, $V = 0$ V. It's worth noting that the plots for non-zero voltage are in

	distinguishable from that of $V = 0$ V, since the application of transverse voltage does not induce any accumulated charges at the interface with the vacuum.	81
Figure 5.2	The curves $R(\lambda), \phi_R(\lambda), T(\lambda)$, and $\phi_T(\lambda)$ for a non-obliquely incident electromagnetic wave, $\theta_0 = 0^\circ$. These curves have been synthesized using the WT-II code when implementing a $V = 0, 300, 600$, and 900 V transverse electrical potentials on a bi-layer thin film composed of germanium (Ge) and magnesium oxide (MgO), where the combined thickness equals 2×36.293 nm.	82
Figure 5.3	The curves $R(\lambda), \phi_R(\lambda), T(\lambda)$, and $\phi_T(\lambda)$ for a non-obliquely incident electromagnetic wave, $\theta_0 = 0^\circ$. These curves have been synthesized using the WT-II code when implementing a $V = 0, 300, 600$, and 900 V transverse electrical potentials on a tri-layer thin film comprising germanium (Ge), magnesium oxide (MgO), and another layer of germanium (Ge), where the combined thickness equals 3×36.293 nm.	83
Figure 5.4	The curves $R(\lambda), \phi_R(\lambda), T(\lambda)$, and $\phi_T(\lambda)$ for a non-obliquely incident electromagnetic wave, $\theta_0 = 0^\circ$. These curves have been synthesized using the WT-II code when implementing a $V = 0, 300, 600$, and 900 V transverse electrical potentials on a thin film consisting of four layers, with alternating layers of Ge and MgO, where the combined thickness equals 4×36.293 nm.	84
Figure 5.5	The curves $R(\lambda), \phi_R(\lambda), T(\lambda)$, and $\phi_T(\lambda)$ for a non-obliquely incident electromagnetic wave, $\theta_0 = 0^\circ$. These curves have been synthesized using the WT-II code when implementing a $V = 0, 300, 600$, and 900 V transverse electrical potentials on a thin film consisting of five layers, with alternating layers of Ge and MgO, where the combined thickness equals 5×36.293 nm.	85

- Figure 5.6 The curves $R(\lambda), \phi_R(\lambda), T(\lambda)$, and $\phi_T(\lambda)$ for a non-obliquely incident electromagnetic wave, $\theta_0 = 0^\circ$. These curves have been synthesized using the WT-II code when implementing $V = 0, 300, 600$, and 900 V transverse electrical potentials on a thin film consisting of six layers, with alternating layers of Ge and MgO, where the combined thickness equals 6×36.293 nm.86
- Figure 5.7 The curves $R(\lambda), \phi_R(\lambda), T(\lambda)$, and $\phi_T(\lambda)$ that have been synthesized using the WT-II code for a non-obliquely incident electromagnetic wave, $\theta_0 = 0^\circ$. These curves have been obtained without applying any transverse electrical potential on a thin film consisting of N layers, with alternating layers of Ge and MgO, for $N \in 1, 3, 5$87
- Figure 5.8 The curves $R(\lambda), \phi_R(\lambda), T(\lambda)$, and $\phi_T(\lambda)$ that have been synthesized using the WT-II code for a non-obliquely incident electromagnetic wave, $\theta_0 = 0^\circ$. These curves have been obtained without applying any transverse electrical potential on a thin film consisting of N layers, with alternating layers of Ge and MgO, for $N \in 2, 4, 6$88
- Figure 5.9 The curves $R(\lambda), \phi_R(\lambda), T(\lambda)$, and $\phi_T(\lambda)$ that have been synthesized using the WT-II code for a non-obliquely incident electromagnetic wave, $\theta_0 = 0^\circ$. These curves have been obtained by implementing a $V = 300$ V transverse electrical potential on a thin film consisting of N layers, with alternating layers of Ge and MgO, for $N \in 1, 3, 5$89
- Figure 5.10 The curves $R(\lambda), \phi_R(\lambda), T(\lambda)$, and $\phi_T(\lambda)$ that have been synthesized using the WT-II code for a non-obliquely incident electromagnetic wave, $\theta_0 = 0^\circ$. These curves have been obtained by implementing a $V = 300$ V transverse electrical potential on a

	thin film consisting of N layers, with alternating layers of Ge and MgO, for $N \in 2,4,6$	90
Figure 5.11	The curves $R(\lambda), \phi_R(\lambda), T(\lambda)$, and $\phi_T(\lambda)$ that have been synthesized using the WT-II code for a non-obliquely incident electromagnetic wave, $\theta_0 = 0^\circ$. These curves have been obtained by implementing a $V = 600$ V transverse electrical potential on a thin film consisting of N layers, with alternating layers of Ge and MgO, for $N \in 1,3,5$	91
Figure 5.12	The curves $R(\lambda), \phi_R(\lambda), T(\lambda)$, and $\phi_T(\lambda)$ that have been synthesized using the WT-II code for a non-obliquely incident electromagnetic wave, $\theta_0 = 0^\circ$. These curves have been obtained by implementing a $V = 600$ V transverse electrical potential on a thin film consisting of N layers, with alternating layers of Ge and MgO, for $N \in 2,4,6$	92
Figure 5.13	The curves $R(\lambda), \phi_R(\lambda), T(\lambda)$, and $\phi_T(\lambda)$ that have been synthesized using the WT-II code for a non-obliquely incident electromagnetic wave, $\theta_0 = 0^\circ$. These curves have been obtained by implementing a $V = 900$ V transverse electrical potential on a thin film consisting of N layers, with alternating layers of Ge and MgO, for $N \in 1,3,5$	93
Figure 5.14	The curves $R(\lambda), \phi_R(\lambda), T(\lambda)$, and $\phi_T(\lambda)$ that have been synthesized using the WT-II code for a non-obliquely incident electromagnetic wave, $\theta_0 = 0^\circ$. These curves have been obtained by implementing a $V = 900$ V transverse electrical potential on a thin film consisting of N layers, with alternating layers of Ge and MgO, for $N \in 2,4,6$	94
Figure 5.15	The curves $R(\lambda), \phi_R(\lambda), T(\lambda)$, and $\phi_T(\lambda)$ that have been synthesized using the WT code for an obliquely incident	

	electromagnetic wave at an angle of $\theta_0 = \theta_B (\text{MgO})$. These curves were obtained without applying transverse electrical potential to a one-layer MgO film.....	98
Figure 5.16	The curves $R(\lambda), \phi_R(\lambda), T(\lambda)$, and $\phi_T(\lambda)$ that have been synthesized using the WT code for an obliquely incident electromagnetic wave at an angle of $\theta_0 = \theta_B (\text{MgO})$. These curves have been obtained by implementing $V = 0, 300, 600$, and 900 V transverse electrical potentials on a bi-layer thin film composed of magnesium oxide (MgO) and calcium fluoride (CaF_2), where the combined thickness equals $2 \times 36.293 \text{ nm}$	99
Figure 5.17	The curves $R(\lambda), \phi_R(\lambda), T(\lambda)$, and $\phi_T(\lambda)$ that have been synthesized using the WT code for an obliquely incident electromagnetic wave at an angle of $\theta_0 = \theta_B (\text{MgO})$. These curves have been obtained by implementing $V = 0, 300, 600$, and 900 V transverse electrical potentials on tri-layer thin film comprising magnesium oxide (MgO), calcium fluoride (CaF_2), and another layer of magnesium oxide (MgO), where the combined thickness equals $3 \times 36.293 \text{ nm}$	100
Figure 5.18	The curves $R(\lambda), \phi_R(\lambda), T(\lambda)$, and $\phi_T(\lambda)$ that have been synthesized using the WT code for an obliquely incident electromagnetic wave at an angle of $\theta_0 = \theta_B (\text{MgO})$. These curves have been obtained by implementing $V = 0, 300, 600$, and 900 V transverse electrical potentials on a thin film consisting of four layers, with alternating layers of MgO and CaF_2 , where the combined thickness equals $4 \times 36.293 \text{ nm}$	101
Figure 5.19	The curves $R(\lambda), \phi_R(\lambda), T(\lambda)$, and $\phi_T(\lambda)$ that have been synthesized using the WT code for an obliquely incident electromagnetic wave at an angle of $\theta_0 = \theta_B (\text{MgO})$. These curves	

have been obtained by implementing $V = 0, 300, 600$, and 900 V transverse electrical potentials on a thin film consisting of five layers, with alternating layers of MgO and CaF₂, where the combined thickness equals 5×36.293 nm. 102

Figure 5.20 The curves $R(\lambda), \phi_R(\lambda), T(\lambda)$, and $\phi_T(\lambda)$ that have been synthesized using the WT code for an obliquely incident electromagnetic wave at an angle of $\theta_0 = \theta_B(\text{MgO})$. These curves have been obtained without implementing any transverse electrical potential on a thin film consisting of N layers with alternating layers of MgO and CaF₂, for $N \in 1, 2, 3, 4, 5$ 103

Figure 5.21 The curves $R(\lambda), \phi_R(\lambda), T(\lambda)$, and $\phi_T(\lambda)$ that have been synthesized using the WT code for an obliquely incident electromagnetic wave at an angle of $\theta_0 = \theta_B(\text{MgO})$. These curves have been obtained by implementing a $V = 300$ V transverse electrical potential of on a thin film consisting of N layers with alternating layers of MgO and CaF₂, for $N \in 1, 2, 3, 4, 5$ 104

Figure 5.22 The curves $R(\lambda), \phi_R(\lambda), T(\lambda)$, and $\phi_T(\lambda)$ that have been synthesized using the WT code for an obliquely incident electromagnetic wave at an angle of $\theta_0 = \theta_B(\text{MgO})$. These curves have been obtained by implementing a $V = 600$ V transverse electrical potential of on a thin film consisting of N layers with alternating layers of MgO and CaF₂, for $N \in 1, 2, 3, 4, 5$ 105

Figure 5.23 The curves $R(\lambda), \phi_R(\lambda), T(\lambda)$, and $\phi_T(\lambda)$ that have been synthesized using the WT code for an obliquely incident electromagnetic wave at an angle of $\theta_0 = \theta_B(\text{MgO})$. These curves have been obtained by implementing a $V = 900$ V transverse electrical potential on a thin film consisting of N layers with alternating layers of MgO and CaF₂, for $N \in 1, 2, 3, 4, 5$ 106

- Figure 5.24 The curves $R(\lambda), \phi_R(\lambda), T(\lambda)$, and $\phi_T(\lambda)$ that have been synthesized using the WT code for a non-obliquely incident electromagnetic wave, i.e., $\theta_0 = 0^\circ$. These curves have been obtained when implementing $V = 0, 300, 600, 900$ V transverse electrical potentials on a bi-layer thin film composed of Calcium fluoride (CaF_2) and silicon dioxide (SiO_2), where the combined thickness equals 2×36.293 nm. 109
- Figure 5.25 The curves $R(\lambda), \phi_R(\lambda), T(\lambda)$, and $\phi_T(\lambda)$ that have been synthesized using the WT code for a non-obliquely incident electromagnetic wave, i.e., $\theta_0 = 0^\circ$. These curves have been obtained when implementing $V = 0, 300, 600, 900$ V transverse electrical potentials on a tri-layer thin film composed of Calcium fluoride (CaF_2), silicon dioxide (SiO_2), and another layer of Calcium fluoride (CaF_2), where the combined thickness equals 3×36.293 nm. 110
- Figure 5.26 The curves $R(\lambda), \phi_R(\lambda), T(\lambda)$, and $\phi_T(\lambda)$ that have been synthesized using the WT code for a non-obliquely incident electromagnetic wave, i.e., $\theta_0 = 0^\circ$. These curves have been obtained when implementing a $V = 0, 300, 600$, and 900 V transverse electrical potentials on a thin film consisting of four layers, with alternating layers of CaF_2 and SiO_2 , where the combined thickness equals 4×36.293 nm. 111
- Figure 5.27 The curves $R(\lambda), \phi_R(\lambda), T(\lambda)$, and $\phi_T(\lambda)$ that have been synthesized using the WT code f for a non-obliquely incident electromagnetic wave, i.e., $\theta_0 = 0^\circ$. These curves have been obtained when implementing a $V = 0, 300, 600$, and 900 V transverse electrical potentials on a thin film consisting of twenty-four layers, with alternating layers of CaF_2 and SiO_2 , where the combined thickness equals 24×36.293 nm. 112

Figure A.1	Scattering of an electric field through a sample bounded at z_1 and z_2 . The symbols $E^+(z_1)$, and $E^-(z_1)$ represent incident and reflected wave functions respectively at position z_1 , while $E^+(z_2)$, and $E^-(z_2)$ represent incident and reflected.....	131
Figure D.1	Euler angle rotation about the y-axis through angle θ_i	144

LIST OF ABBREVIATIONS

EM	Electromagnetic
TM	Transverse Magnetic
TE	Transverse Electric
TEM	Transverse-Electric-Magnetic
BCITL	Bi-Characteristic-Impedance Transmission Line
CCITL	Conjugate Characteristic Impedance Transmission Line
PM	Propagation Matrix
IM	Interface Matrix
LED	Light Emitting Diode
PVD	Physical Vapour Deposition
CVD	Chemical Vapour Deposition
WT	Wave Tensor
IPS	Institut Pengajian Siswazah
USM	Universiti Sains Malaysia

LIST OF SYMBOLS

E	Electrical field
B	Magnetic flux density
H	Magnetic field
M	Magnetic polarization or magnetic dipole moment per unit volume
χ_m	Magnetic susceptibility
D	Electrical displacement
P	Electric polarization or electric dipole moment per unit volume
χ_e	Electric susceptibility
ω	Angular frequency
k	Wave number
R	Reflection
ϕ_R	Phase angle of reflection
T	Transmission
ϕ_T	Phase angle of transmission
n	Refractive index
μ	Permeability
μ_0	Permeability of the vacuum
μ_r	Relative permeability
ε	permittivity
$\tilde{\varepsilon}_c$	Complex permittivity
$\tilde{\varepsilon}_{cr}$	Relative complex permittivity
ε_r	Dielectric constant or relative permittivity
σ	Electric conductivity of the material
$\tilde{\sigma}_s$	Surface electric conductivity
J_{total}	Total current density
J_{bound}	Bound current density or displacement current
J_{free}	Free current density
J_{con}	Conduction current density
J_{ext}	Current density due to an external source
J_{pol}	Polarization current density
J_{mag}	Magnetization current density

ρ_{total}	Charge density
ρ_{bound}	Bound charge density
ρ_{pol}	Polarization charge density
ρ_{mag}	Magnetic charge density
ρ_{ext}	Free charge density or external charge density
η	Intrinsic impedance
η_0	Intrinsic impedance of vacuum
Z_j	Impedance of the j^{th} line section in the multi-section model
θ_B	Brewster angle
θ_c	Critical angle
\tilde{r}	Fresnel's reflection coefficient
\tilde{t}	Fresnel's transmission coefficient
m^*	Effective mass of an electron
e	Electron charge
$[A]$	Interface matrix
$[\beta]$	Propagation matrix
$[M]:$	Transfer matrix

LIST OF APPENDICES

Appendix A	Conservation of the current density of EM fields in terms of the transfer matrix $[M]$
Appendix B	Plane-wave in unbounded, homogeneous, isotropic media
Appendix C	The relationships between charge densities and current densities
Appendix D	Transformation of operators $\vec{\nabla}$, $\vec{\nabla} \cdot$, and $\vec{\nabla} \times$ from x, y, z coordination to x', y', z'
Appendix E	Inner product in a complex vector space, or Hermitian inner product
Appendix F	Solution of a second-order homogeneous differential equation for electric time-dependent field and magnetic time-dependent field
Appendix G	Writing Maxwell's equations for a plane wave in an SI system in terms of an electric field, magnetic field, and wave propagation vector as a complex orthogonal set.
Appendix H	Electric and Magnetic field harmonic in time
Appendix I	Deduction of intrinsic impedance formula
Appendix J	Deduction of permittivity formula

**MODEL POLINOMIAL BAGI PENGHANTARAN DAN PANTULAN
GELOMBANG ELEKTROMAGNET DALAM FILEM NIPIS BERBILANG
LAPIS DIKENAKAN SUATU VOLTAN MELINTANG LUARAN**

ABSTRAK

Dalam merekabentuk dan mengawal ciri-ciri penghantaran dan pantulan filem nipis berbilang lapisan, pemodelan matematik terhadap respon elektrik dan optik adalah langkah penting untuk menjimatkan masa, usaha dan wang dalam proses pembuatan eksperimen. Terdapat pelbagai pendekatan yang ada untuk memodelkan penyebaran gelombang elektromagnetik melalui filem nipis pelapis berganda. Tesis ini menggunakan pendekatan polinomial untuk memodelkan gelombang elektromagnetik, dengan menggunakan pemalar dielektrik, rintangan elektrik, dan indeks bias filem nipis untuk menentukan penghantaran dan pantulan dan pantulan gelombang elektromagnetik yang berlaku pada struktur berbilang lapisan apabila satu atau lebih kawasan cas terkumpul disatukan antara lapisan bersebelahan. Model ini, berdasarkan persamaan Maxwell, telah dihasilkan untuk bahan tidak magnetik yang tidak berhilang atau berhilang. Kod WaveTensor dan WaveTensor-II, yang dibangunkan sendiri menggunakan MATLAB, telah digunakan untuk mensimulasikan model polinomial bagi tiga pasang bahan iaitu bahan berhilang tidak magnetik, germanium, dan bahan tidak berhilang tidak magnetik, magnesium oksida. Pasangan kedua terdiri daripada dua bahan tidak berhilang tidak magnetik, magnesium oksida dan kalsium fluorida. Pasangan bahan ketiga juga terdiri daripada dua bahan tidak berhilang tidak magnetik: kalsium fluorida dan silikon dioksida. Pemalar dielektrik, rintangan elektrik, dan indeks bias bahan-bahan yang dipilih telah dicari dari rujukan yang dipercayai. Hasil kod WaveTensor dan WaveTensor-II telah disahkan dengan

menggunakan pemeliharaan ketumpatan arus medan elektromagnetik, ujian sudut kritis, dan ujian sudut Brewster. Pendekatan polinomial telah terbukti dapat dipercayai dan tepat dalam memodelkan pemindahan dan pantulan gelombang elektromagnetik yang terjadi pada filem nipis pelapis berganda yang terdiri daripada bahan tidak magnetik yang tidak berhilang atau berhilang apabila voltan melintang dikenakan pada keseluruhan struktur. Melalui representasi visual dan analisis berangka, kebolehpercayaan dan ketepatan metodologi polinomial sebagai kerangka matematik telah diterangkan untuk menghuraikan tingkah laku penyebaran gelombang elektromagnetik dalam filem nipis pelbagai lapisan. Analisis ini merangkumi skenario yang melibatkan bahan bukanmagnet yang tidak berjangkit dan yang berjangkit, di bawah pengaruh voltan melintang.

**POLYNOMIAL MODEL OF TRANSMISSION AND REFLECTION OF
ELECTROMAGNETIC WAVES IN MULTILAYER THIN FILMS
SUBJECTED TO AN EXTERNAL TRANSVERSE VOLTAGE**

ABSTRACT

In designing and controlling the transmission and reflection characteristics of multilayer thin films, mathematical modelling of their electrical and optical response is a vital step to save time, effort and money in the experimental fabrication process. Different approaches exist for modelling the propagation of electromagnetic waves through multilayer thin films. This thesis employs the polynomial approach to model the electromagnetic wave, utilizing dielectric constants, electrical resistivities, and refractive indices of thin film materials to infer the transmission and reflection of electromagnetic wave incidents on the multilayer structure when one or more accumulated-charge regions superimpose between adjacent layers. The model, based on Maxwell's equations was derived for nonmagnetic lossless or lossy materials. Wave Tensor and Wave Tensor-II, home-grown MATLAB codes, were used to simulate the polynomial model for three pairs of materials: pair consists of a non-magnetic lossy material, germanium, and a non-magnetic lossless material, magnesium oxide. Second pair are two non-magnetic lossless materials, magnesium oxide and calcium fluoride. Third pair of materials are two non-magnetic lossless materials: calcium fluoride and silicon dioxide. The dielectric constants, electrical resistivities, and refractive indices of chosen materials were outsourced from trustworthy references. The results of Wave Tensor and Wave Tensor-II codes were verified using the conservation of EM field current density, critical angle test, and Brewster's angle test. The polynomial approach proved to be reliable and accurate in modelling the transmission and reflection of

electromagnetic waves incident on multilayer thin films consisting of nonmagnetic lossless and lossy materials when applying a transverse voltage to the whole structure. Through visual representations and numerical analysis, the reliability and precision of the polynomial methodology are elucidated as a mathematical framework for characterizing the behaviour of electromagnetic wave propagation in multilayer thin films. This analysis encompasses scenarios involving both nonmagnetic lossless and lossy materials, under the influence of a transverse voltage.

CHAPTER 1

INTRODUCTION

1.1 Motivation

Thin films are a hot topic due to their widespread use in industry and research. In industry, they're used for creating electronic devices, solar cells, and sensors. As technology advances, understanding the optical response of thin films is crucial for producing more efficient, durable, and cost-effective products. In the scientific community, the study of thin films has gained popularity as it provides crucial insights into the fundamental properties of materials and their interaction with light. Researchers are investigating the behaviour of thin films under different conditions, such as oblique incidence, and polarization rotation, to understand the underlying physical mechanisms and optimize the properties of the films. Additionally, thin film research can advance fields such as materials science, physics, and engineering. Scientists are exploring the optical and electronic properties of thin films to enhance the performance of electronic devices, create advanced sensing technologies, and develop more efficient energy storage systems. Continued research into thin films will undoubtedly lead to new and innovative technologies, with potential applications in numerous industries, from electronics and energy to healthcare and communications. By understanding and optimizing the optical properties of thin films, researchers can continue to drive innovation and create products that benefit society as a whole.

1.2 Research Gap

In former studies [1], [2], [3], [4], [5], [6], [7], [8], [9], [10], [11], [12], [13], [14], [15], [16], [17], [18], [19], [20], [21], [22], [23], the retort of electromagnetic waves propagating through slender layers crafted from magnetic, nonmagnetic, lossy, and

lossless substances, and intricate substances akin to metamaterials, meta-surfaces, and photonic crystals, were investigated. These inquiries were undertaken with varying incidence angles, polarization rotations, and wavelengths. Yet the study delved into the outcome of applying a transverse voltage across multilayer thin films on the optical reaction of electromagnetic waves.

1.3 Problem statement

This thesis aims to establish a comprehensive theoretical and computational framework for investigating the interaction of electromagnetic waves with nonmagnetic, lossy, and lossless materials, such as calcium fluoride, magnesium oxide, germanium, and silicon dioxide. Through the utilization of both theoretical and computational approaches, this study seeks to analyse the behaviour of electromagnetic waves in these materials under various conditions, including oblique incidence, polarization rotation, and applying a transverse voltage through multilayer thin films. By developing novel technique in this thesis for manipulating and controlling the properties of these waves, the research aims to contribute to the advancement of the field of photonics, deepen our understanding of the fundamental principles underlying the interaction of light with matter, and enable the development of new and innovative technologies for sensing, imaging, communication, and energy harvesting. The results of this work are expected to have significant implications for the design and optimization of advanced optical systems and devices, as well as for the development of emerging technologies in the field of photonics.

1.4 Objectives

1. To establish a comprehensive theoretical and computational model for exploring complex electromagnetic wave interactions with multilayer thin films under the influence of transverse voltage by developing a computational package, the Wave Tensor Code.
2. To employ the Wave Tensor Code to simulate and analyse the optical response of electromagnetic waves propagating through multilayer thin films, with a specific focus on the influence of transverse voltage.
3. To simulate and analyze, using the Wave Tensor Code, the optical response of electromagnetic waves propagating through multilayer thin films made of isotropic, homogeneous, non-magnetic materials, comparing the behavior of lossless and lossy materials.

1.5 The scope and limitations of work

The thesis delves into the intricate realm of specific formulas, calculating the transmission and reflection coefficients of Fresnel. These formulas, in essence, depend on the refractive index and extinction coefficient. The general formulas of Fresnel's coefficients are expressed in terms of intrinsic impedance. However, due to the paucity of a comprehensive database of intrinsic impedance for materials across a wide range of wavelengths, as opposed to the abundance of databases for refractive index and extinction coefficient for most materials, we are restricted to dealing with nonmagnetic materials. The mathematical and physical derivation of the Fresnel transmission and reflection coefficients as a function of refractive index and extinction coefficients from the general formulas written as a function of intrinsic impedance is thoroughly discussed in subsections 3.3 and 3.4 for TM and TE modes, respectively, in the case of lossy materials. Additionally, the discussion of these coefficients for lossless

materials is presented in subsections 3.5 and 3.6 for TM and TE modes, respectively. The simulation of electromagnetic wave propagation through thin film layers in this thesis relies on the Wave Tensor code and Wave Tensor-II code. However, limitations exist in the use of these codes. Specifically, the Wave Tensor code is limited to the simulation of isotropic, homogeneous, non-magnetic lossless materials and relies solely on the refractive index. On the other hand, Wave Tensor-II code is limited to isotropic, homogeneous, non-magnetic lossy materials and requires both the refractive index and extinction coefficient. Both codes incorporate the application of transverse voltage on the thin film to simulate the reflection and transmission of electromagnetic waves.

1.6 Contribution of the dissertation

The thesis has developed a mathematical model to elucidate the optical response of electromagnetic waves through multilayer thin films crafted of nonmagnetic, lossy, and lossless materials subject to fluctuating transverse voltages. By means of the Wave Tensor, a code of our own making, we did simulate the model and received outputs to wit: transmission, transmission phase angle, reflection, and reflection phase angle, as they do vary by wavelength. Three modes of verification were applied to the code, to ensure its veracity and soundness. This is the initial study to delve into the effects of transverse voltage on electromagnetic waves through multilayer thin films. The theoretical and computational framework presented in this thesis may stir novel optical inventions and contrivances.

1.7 Thesis outline and organization

Chapter One serves as the gateway to this dissertation, offering a glimpse into the motivation that led to its inception. It is here that the research gap is identified, and the

problem statement is defined, providing a clear understanding of the purpose of this study. This chapter also outlines the objectives and the scope and limitations of the work, giving readers an idea of what to expect from the rest of the dissertation.

Moreover, Chapter one introduces the contribution of this research, shedding light on how it will advance the field of optics and inspire further research in the future. The thesis outline and organization are also presented in this chapter, providing a roadmap for readers to follow as they navigate through the dissertation. With this comprehensive introduction, readers will be equipped with the necessary background knowledge to fully appreciate the following chapters and the contributions they make to the field.

Chapter two, literature review, summarizes the technique of making thin films empirically and discusses its applications in various industries. It also covers the various mathematical models used to model electromagnetic wave propagation in multilayer thin films. The chapter emphasizes the importance of theoretical study and computational simulation as a preliminary phase to experimental work.

In chapter three, the theory chapter, the modelling techniques utilized to analyse the interactions between electromagnetic waves and multilayer structures are presented in detail. The chapter delves into the modelling of EM interactions with a multilayer structure using the polynomial method, emphasizing the mathematical expressions of the electric field and magnetic field as column vectors. This enables a clear understanding of the implementation of the interface matrix and propagation matrix of the multilayer thin films. To analyse the interactions between EM waves and multilayer structures, Fresnel's coefficients are derived for both types of polarized EM waves, transverse magnetic mode (P-polarized) and transverse electric mode (S-polarized), for both lossy and lossless nonmagnetic mediums. This chapter also

explores the impact of applying a transverse voltage across thin films and derives new formulas for Fresnel's reflection and transmission coefficients, which are thoroughly discussed. The new formulas are elaborated to modify the polynomial approach, specifically the interface matrix between the adjacent layers, leading to a comprehensive understanding of the EM interactions with multilayer structures. Furthermore, this chapter includes a comparison of the newly derived formulas with existing literature to verify their accuracy and reliability. The appendices of this chapter are not to be underestimated, for they serve as the cornerstone of the mathematical derivations presented here. The reader must consult these appendices to fully grasp the concepts that are being discussed. Without them, the mathematical manipulations may seem ambiguous and hard to follow. In addition to serving as a starting point for the mathematical derivations, the appendices also contain valuable information on the physical properties of the materials used in the fabrication of thin films. These properties play a crucial role in determining the behaviour of electromagnetic waves within the thin films. Moreover, the appendices provide insights into the various fabrication techniques used to deposit thin films onto substrates. Each technique has its advantages and disadvantages, and the choice of technique depends on the desired properties of the thin film and the substrate. Understanding these techniques is crucial for ensuring the reproducibility of the experiments and the consistency of the results. Overall, the appendices are an essential component of this chapter, and the reader should not skip over them. They provide the necessary foundation for the mathematical derivations and offer valuable insights into the physical properties and fabrication techniques of thin films. The theoretical framework presented in this chapter may pave the way for the development of innovative optical devices and applications.

In Chapter Four, which is the Methodology chapter, the readers are presented with a comprehensive explanation of the data sources and the methodology used in the research. The chapter dives into the details of the data collection process and the instruments used to obtain them. The data obtained are then fed into the Wave Tensor code, which is a custom-built tool that enables researchers to simulate and analyse electromagnetic wave propagation through multilayer thin films. To ensure the accuracy and reliability of the results obtained from the Wave Tensor code, various means of verification have been employed. The first one is the conservation of current density, which is an important concept in electromagnetic wave propagation. The second means of verification is the Brewster angle, which describes the angle at which the reflected light is completely polarized. Lastly, the critical angle, which is the minimum angle of incidence at which total internal reflection occurs, is used as another means of verification. The chapter delves into the mathematical details of these means of verification and how they have been compared with the simulated output resulting from the Wave Tensor code. This is an essential step in the validation and robustness of the methodology used in the research. Through this chapter, readers can gain a better understanding of the methodology and the tools used to obtain the results presented in the research.

In Chapter Five, the results and discussions are presented in detail. The simulated results for a carefully chosen set of multilayer thin film structures are showcased in this chapter. The selected thin films are all made of nonmagnetic materials, as the polynomial approach utilized for this study is limited to these materials. The selected materials include lossy materials such as germanium, as well as lossless materials such as magnesium oxide, calcium fluoride, and silicon dioxide. The simulation results were generated using Wave Tensor while applying various values of transverse voltages to

the thin films. The chapter is enriched with an array of figures, each presenting a unique set of results. These figures help to present the output in a visually appealing manner and ease the comparison between different sets of results. The discussion in Chapter Five is not limited to the presentation of the results. It also delves deeper into the interpretation of the results and provides insights into the behaviour of electromagnetic waves when propagating through multilayer thin films. The chapter concludes with a critical evaluation of the findings, highlighting their significance and potential implications for future research in this field.

The concluding chapter of this thesis serves as the final destination of this academic journey. It summarises the main findings and contributions of the study, highlighting the significance of the research in the field of thin film technology. The results of this study demonstrate that the use of the home-grown code, Wave Tensor, is an efficient tool for modelling the propagation of electromagnetic waves through multilayer thin films. Furthermore, this thesis has shed light on the importance of theoretical study and computational simulation as a phase that precedes experimental work. The suggested future work in this field includes the exploration of magnetic materials and the improvement of the polynomial approach to model their behaviour.

CHAPTER 2

LITERATURE REVIEW

Multilayer thin films are a fascinating area of study in materials science. As the name suggests, these films consist of multiple layers of material. Multilayer thin films have a long and fascinating history. The multilayer thin film is an arrangement of two or more layers synthesized by the deposition of dissimilar materials one over another. The thickness of thin film ranges from fractions of a nanometer to several micrometers. They are created through a process called thin film deposition, which involves depositing the layers of material onto a substrate using various techniques [20], [24], [25]. The concept of depositing multiple layers of material onto a substrate to create a thin film date back to the early 20th century. In the 1920s and 1930s, scientists began experimenting with different techniques for depositing thin films, including sputtering and evaporation [26], [27], [28], [29], [30], [31], [32], [33]. Multilayer thin films have unique physical and chemical properties that make them useful in a wide range of applications. By the 1950s, multilayer thin films were being used in a variety of applications, including electronics and optics. However, it wasn't until the 1980s that the field really took off. Advances in technology, such as ion beam assisted deposition and molecular beam epitaxy, made it possible to create thin films with incredibly precise properties.

Thin films can be deposited onto a substrate using a variety of techniques, including physical vapour deposition (PVD) [34], [35], [36], [37], chemical vapour deposition (CVD) [38], [39], [40], [41], electroplating [42], [43], [44], and spin coating [45], [46], [47], [48]. The choice of deposition technique depends on the desired properties of the thin film and the substrate [20], [24], [25], [26], [27], [28]. One important property of thin films is their structural quality, which can be influenced by the deposition

technique, substrate temperature, and other process parameters [23], [49], [50], [51], [52]. Another important property is the chemical composition of the thin film, which can be controlled by using different process conditions during deposition. The development of thin-film fabrication technology [1], [53] eases the study of materials with novel and unique characteristics and is employed in numerous innovations such as thin-film solar cells [2], [5], [10], [14], [54], thin-film batteries [3], [7], [55], [56], LEDs (light emitting diode) [16], [57], [58], semiconductor devices [16], [57], [58], integrated circuits [4], [8], [13], [59], and magnetic recording media [60], [61], [62], [63]. The artificial design of multilayer thin films supplies considerable opportunities to tune the optical responses of EM waves incident upon their surface at an angle. Two basic optical responses are relevant to practical applications, namely reflection and transmission [64], [65], [66]. There are many challenges in the synthesis and processing of thin films, including the need to control the microstructure, thickness, and composition of the film. In addition, there is a need to understand how the properties of the thin film are influenced by the type of materials and the interface between layers. Theoretical design and study of the electrical and optical responses of multilayer thin films is an important phase that precedes the experimental phase and saves time, money, and effort various theoretical approaches can be used to design and study the electrical and optical responses of multilayer thin films [6], [12], [22], [67], [68]. These include analytical models, numerical simulations, and first-principles calculations [29]. These approaches can be used to predict film properties and understand the underlying physical mechanisms. One important aspect of the electrical response of multilayer thin films is the conductivity, which can be influenced by the presence of defects, impurities, and accumulated charge between the layers. The optical response of multilayer thin films is figured out by the absorption, the scattering,

and the reflection of light, which can be influenced by the refractive index, extinction coefficient, and the thickness and shape of the layers. The electrical characteristics and the optical properties of thin films are closely intertwined. Depending on the constituent materials' physical properties and the thin film's shape, the number and thickness of layers, the optical responses can be predicted.

2.1 Modelling of EM interactions with a multilayer structure

Propagation of electromagnetic wave through multilayer thin films may be analyzed with the Transfer Matrix Method, one of the widely used mathematical methods [69], [70], [71], [72], [73], [74], [75]. The polynomial approach is the preferable mathematical technique when tracing the electromagnetic vector layer by layer [76], [77], [78], [79], [80], [81], [82], [83], [84]. For modelling the ray beam or the Gaussian beam then the ray transfer matrix is a suitable choice [85], [86], [87], [88]. Propagator dyadic can effectively model EM wave propagates through inhomogeneous planar layered media [89], [90], [91], [92], [93], [94], [95]. The conjugate characteristic impedance transmission line and the bi-characteristic-impedance transmission line are both mathematical models that emerged from the transmission line theory and were used to study the lossless and lossy transmission lines, respectively. Physicists employed these two models in studying optical transmission and reflection for multilayer structures [1], [10], [14], [23], [50], [51], [52], [53], [54]. Solving Maxwell's equations for the band structure [96], [97] of specific photonic crystal geometries or inhomogeneous materials using plane wave expansion is a popular method [98], [99], [100], [101], [102], [103], [104]. One of the most used methods to solve the time-dependent Maxwell equations is the finite difference time domain [105], [106], [107], [108], [109], [110], [111].

2.2 Transfer matrix

A transfer matrix is a well-known and successful way to represent and analyze an optical-electrical system or device mathematically [69], [70], [74], [75], [108], [112].

The thin film of an arbitrary number of layers, N , that are arranged to form a multilayer thin film structure is indexed using an indexing scheme, $j \in [1, 2, \dots, N]$. The first layer is labelled as $j = 1$, so the amplitude of the electric field at the edge of the left boundary of the first layer, at $z = z_1$ is written as

$$\tilde{E}^\pm(z = z_1) = \begin{bmatrix} \tilde{E}^+(z_1) \\ \tilde{E}^-(z_1) \end{bmatrix}, \quad 2.2.1$$

where the forward electric field, $\tilde{E}^+(z_1)$, is taken as the incident field at $z = z_1$. The backward electric field, $\tilde{E}^-(z_1)$, is taken as the reflected electric field at $z = z_1$. While the amplitude of the electric field at the edge of the right boundary of the last layer, at $z = z_{N+1}$ is written as

$$\tilde{E}^\pm(z = z_{N+1}) = \begin{bmatrix} \tilde{E}^+(z_{N+1}) \\ \tilde{E}^-(z_{N+1}) \end{bmatrix}. \quad 2.2.2$$

$\tilde{E}^+(z_{N+1})$ is the transmitted electric field at $z = z_{N+1}$. $\tilde{E}^-(z_{N+1})$ is the reflected electric field at $z = z_{N+1}$. The transfer matrix mathematically relates $\tilde{E}^\pm(z = z_1)$ and $\tilde{E}^\pm(z = z_{N+1})$ via the following equation,

$$\begin{bmatrix} \tilde{E}^+(z_{N+1}) \\ \tilde{E}^-(z_{N+1}) \end{bmatrix} = \begin{pmatrix} M_{1,1} & M_{1,2} \\ M_{2,1} & M_{2,2} \end{pmatrix} \begin{bmatrix} \tilde{E}^+(z_1) \\ \tilde{E}^-(z_1) \end{bmatrix}. \quad 2.2.3$$

The equation can be written, for brevity, as $\tilde{E}^\pm(z = z_{N+1}) = M \tilde{E}^\pm(z = z_1)$. Since the wave switches from the last layer N to the vacuum at the boundary $z = z_N + 1$, there is no reflected electric field at $z = z_{N+1}$, $E^-(z_{N+1}) = 0$.

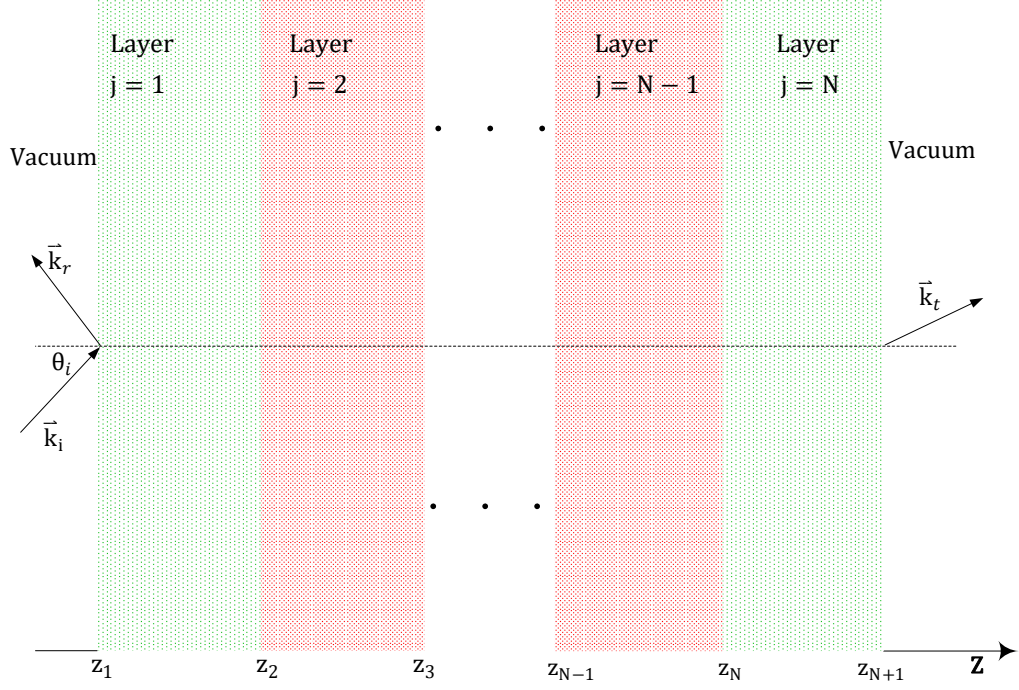


Figure 2.1 Propagation of a plane electromagnetic wave through a multilayer thin film consists of N layers. Propagation of the electric field is from the left boundary at $z = z_1$ to the right boundary at $z = z_{N+1}$

The reflection of the complete system, the N -layer thin film, is defined as the ratio of the amplitude of the backward electric field at $z = z_1$ to the amplitude of the forward electric field at $z = z_1$, while the transmission of the system is defined as the ratio of the amplitude of the forward electric field at $z = z_{N+1}$ to the amplitude of the forward electric field at $z = z_1$, as per

$$\tilde{R} = \frac{\tilde{E}^-(z_1)}{\tilde{E}^+(z_1)} = -\frac{M_{2,1}}{M_{2,2}}, \quad 2.2.4$$

$$\tilde{T} = \frac{\tilde{E}^+(z_{N+1})}{\tilde{E}^+(z_1)} = \frac{\det([M])}{M_{2,2}}, \quad 2.2.5$$

where the reflection \tilde{R} has a magnitude, R , and a phase angle, ϕ_R . Similarly, the transmission \tilde{T} has a magnitude of T and a phase angle of ϕ_T . The magnitude and the phase angle of both reflection and transmission are defined as per

$$R = \sqrt{[\text{Re}(\tilde{R})]^2 + [\text{Im}(\tilde{R})]^2}, \quad 2.2.6$$

$$\phi_R = \tan^{-1} \left(\frac{\text{Im}(\tilde{R})}{\text{Re}(\tilde{R})} \right), \quad 2.2.7$$

$$T = \sqrt{[\text{Re}(\tilde{T})]^2 + [\text{Im}(\tilde{T})]^2}, \quad 2.2.8$$

$$\phi_T = \tan^{-1} \left(\frac{\text{Im}(\tilde{T})}{\text{Re}(\tilde{T})} \right). \quad 2.2.9$$

2.3 ABCD matrix

One of the famous, oldest, and most effective methods in geometrical optics to describe the optical element is an ABCD matrix, which is also known as a “ray transfer matrix” [78]-[81], [106]. ABCD matrix is a mathematical model which can describe the propagation of both the ray beam and the Gaussian beam. The ray transfer matrix is applicable under a paraxial approximation condition. The paraxial approximation assumes that the angle “ θ ” between propagation rays and some reference axis of the optical system always remains small, $\theta \ll 1$ rad, therefore $\tan \theta \approx \sin \theta \approx \theta$. The ray transfer matrix is a 2×2 matrix which describes the linear relationship between the r and θ coordinates before and after an optical element,

$$\begin{bmatrix} r' \\ \theta' \end{bmatrix} = \begin{pmatrix} A & B \\ C & D \end{pmatrix} \begin{bmatrix} r \\ \theta \end{bmatrix}, \quad 2.3.1$$

where r, θ denote the transverse offset and offset angle before the optical element respectively, while r', θ' are the transverse offset and offset angle after the optical element, respectively. The transverse offset is measured with reference to a predetermined optical reference “horizontal line” and the offset angle is an angle formed between the incident ray and the norm line on the optical element, see Figure

2.2. The determinant of an ABCD matrix is the input refractive index divided by the output refractive index,

$$|M| = (AD - BC) = \frac{n}{n'}. \quad 2.3.2$$

When the input refractive index and the output refractive index are the same, then $|M| = 1$.

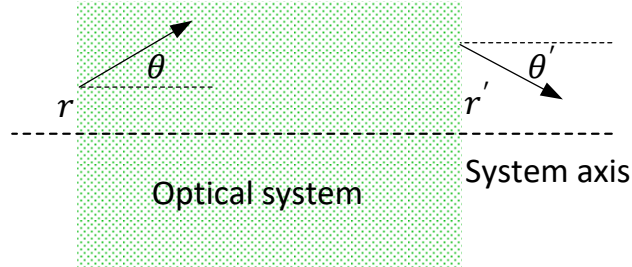


Figure 2.2 Definition of the transverse offset and offset angle before and after the optical system.

When beams propagate through dielectric media, it is convenient to use a modified beam vector, where the angle is multiplied by the refractive index, i.e.,

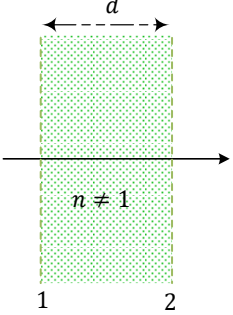
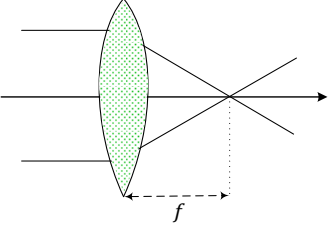
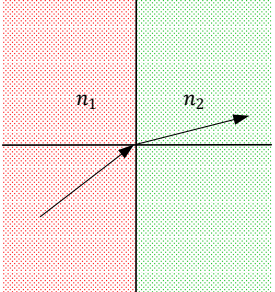
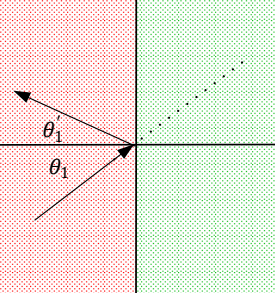
$$\begin{bmatrix} r' \\ n'\theta' \end{bmatrix} = \begin{pmatrix} A & B \\ C & D \end{pmatrix} \begin{bmatrix} r \\ n\theta \end{bmatrix}. \quad 2.3.3$$

The ABCD matrix with the modified beam vector is more general. Examples of important optical elements with their ray transfer matrix are listed in Table 2.1.

Table 2.1 illustrates a small optical element sketch, and an ABCD matrix expression for:

- Propagation of light over distance d on a medium of refractive index n .
- Incidence of light on a thin lens with a focal length “ f ”.
- Refraction of light through a different medium, n_1 and n_2 .
- Reflection of light from a flat mirror.

Table 2.1 A ray transfer matrix for basic optical elements.

Optical Element	ABCD matrix	Illustration of the element
Propagation over distance d on a medium of refractive index n	$\begin{pmatrix} 1 & d/n \\ 0 & 1 \end{pmatrix}$	
A thin lens with a focal length “ f ”	$\begin{pmatrix} 1 & 0 \\ -1/f & 1 \end{pmatrix}$	
Refraction through a different medium	$\begin{pmatrix} 1 & 0 \\ 0 & \frac{n_1}{n_2} \end{pmatrix}$	
Reflection from a flat mirror	$\begin{pmatrix} 1 & 0 \\ 0 & 1 \end{pmatrix}$	

2.4 Propagator matrix

The propagator matrix or propagator dyadic is one of the mathematical models used to study the scattering of the wave from inhomogeneous planar layered media. Dyadic is a second-order tensor [89], [90], [91], [92], [93]. The derivation and the solution of the state equation can be found in [90], [91], [92], [93], [94],

$$\frac{d}{dz} \vec{V} = \vec{D} \vec{V}, \quad 2.4.1$$

where $\vec{\tilde{V}}$ and $\vec{\tilde{D}}$ are the state vector and fundamental dyadic of the medium, respectively. Components of both the state vector and fundamental dyadic can be complex numbers, denoted by the tilde, “ \sim ”. For EM planner wave propagates in the +z direction the state vector can be defined in terms of transverse field components of $\vec{\tilde{E}}$, and $\vec{\tilde{H}}$,

$$\vec{\tilde{V}}(z) = \begin{bmatrix} \tilde{E}_x(z) \\ \tilde{E}_y(z) \\ \tilde{H}_x(z) \\ \tilde{H}_y(z) \end{bmatrix}. \quad 2.4.2$$

Fundamental dyadic, $\vec{\tilde{D}}$, is a 4×4 transition tensor. The component of dyadic is as given in [95]. The general solution of Eq. 2.4.1 is written in Eq. 2.4.3. The derivation of the general solution of the state equation is given in [90],

$$\vec{\tilde{V}}(z) = \vec{\tilde{a}} e^{i\vec{\tilde{\beta}} z} \vec{\tilde{A}}, \quad 2.4.3$$

where $\vec{\tilde{a}}$ is a 4×4 matrix, each component of $\vec{\tilde{a}}$ is an eigenvector, $\vec{\tilde{a}}_j$, $j \in \{1,2,3,4\}$ corresponding to a specific layer i.e.,

$$\vec{\tilde{a}} = [\vec{\tilde{a}}_1 \quad \vec{\tilde{a}}_2 \quad \vec{\tilde{a}}_3 \quad \vec{\tilde{a}}_4]. \quad 2.4.4$$

$\vec{\tilde{\beta}}_z$ is a 4×4 diagonal matrix, each diagonal component of $\vec{\tilde{\beta}}$ correspondences to the j^{th} eigenvalue, and is expressed as

$$e^{i\vec{\tilde{\beta}} z} = \begin{bmatrix} e^{i\beta_1 z} & 0 & 0 & 0 \\ 0 & e^{i\beta_2 z} & 0 & 0 \\ 0 & 0 & e^{-i\beta_3 z} & 0 \\ 0 & 0 & 0 & e^{-i\beta_4 z} \end{bmatrix}. \quad 2.4.5$$

$\vec{\tilde{A}}$ is a column vector with \tilde{A}_j element corresponding to the j^{th} layer.

The eigenvectors matrix and eigenvalues matrix in Eq. 2.4.3 can be ordered to describe multilayer structures of N layers, such that the first pair of matrices correspond to the last layer, $j = N$, while the second pair of “eigenvectors- eigenvalues” matrices correspond to the incident “first layer, $j = 1$ as

$$\begin{aligned}\vec{\tilde{V}}(z_1) &= \bar{a} e^{i\bar{\beta}(z_1 - z_{N+1})} \bar{a}^{-1} \bar{a} e^{i\bar{\beta}(z_{N+1})} \vec{\tilde{A}}, \\ \vec{\tilde{V}}(z_1) &= \vec{\tilde{P}} \vec{\tilde{V}}(z_{N+1}),\end{aligned}\tag{2.4.6}$$

were

$$\vec{\tilde{P}} = \bar{a} e^{i\bar{\beta}(z_1 - z_{N+1})} \bar{a}^{-1}.\tag{2.4.7}$$

An oblique incidence of a TM/TE electromagnetic wave on a multilayer structure, made up of N layers, is depicted in Figure 2.1. The incident angle is θ_0 , each layer has a thickness of d_j , a permeability of μ_j , a permittivity ϵ_j , an intrinsic impedance of η_j , and a wavenumber of k_j , where $j = 0, \dots, N$. The propagator matrix (propagator dyadic) which describes the relationship between the electric field in layer j and layer $j + 1$ is described by $\vec{\tilde{E}}^\mp(z_j) = [\vec{\tilde{P}}]_j \vec{\tilde{E}}^\mp(z_{j+1})$ and written in matrix form as

$$\begin{bmatrix} \vec{\tilde{E}}^- \\ \vec{\tilde{E}}^+ \end{bmatrix}_j = [\vec{\tilde{P}}]_j \begin{bmatrix} \vec{\tilde{E}}^- \\ \vec{\tilde{E}}^+ \end{bmatrix}_{j+1}.\tag{2.4.8}$$

The propagator matrix of the layer j is mathematically expressed

$$\begin{aligned}[\vec{\tilde{P}}]_j &= \frac{1}{2} \begin{bmatrix} \frac{1 + \mu_j k_{z_{j+1}} \cos \theta_{j+1}}{\mu_{j+1} k_{z_j} \cos \theta_j} e^{+i z_j (k_{z_{j+1}} \cos \theta_{j+1} - k_{z_j} \cos \theta_j)} & \frac{1 - \mu_j k_{z_{j+1}} \cos \theta_j}{\mu_{j+1} k_{z_j} \cos \theta_j} \\ \frac{1 - \mu_j k_{z_{j+1}} \cos \theta_{j+1}}{\mu_{j+1} k_{z_j} \cos \theta_j} e^{+i z_j (k_{z_{j+1}} \cos \theta_{j+1} + k_{z_j} \cos \theta_j)} & \frac{1 + \mu_j k_{z_{j+1}} \cos \theta_j}{\mu_{j+1} k_{z_j} \cos \theta_j} \end{bmatrix}.\end{aligned}\tag{2.4.9}$$

The total propagator matrix, of N layers, is defined as follows

$$[\vec{\tilde{P}}] = [\vec{\tilde{P}}]_0 [\vec{\tilde{P}}]_1 [\vec{\tilde{P}}]_2 \dots [\vec{\tilde{P}}]_{N-3} [\vec{\tilde{P}}]_{N-2} [\vec{\tilde{P}}]_{N-1} \equiv \begin{bmatrix} \vec{\tilde{P}}_{1,1} & \vec{\tilde{P}}_{1,2} \\ \vec{\tilde{P}}_{2,1} & \vec{\tilde{P}}_{2,2} \end{bmatrix}.\tag{2.4.10}$$

The total reflection is defined as

$$\tilde{R} = \frac{\vec{\tilde{E}}_0^-}{\vec{\tilde{E}}_0^+} = \frac{\vec{\tilde{P}}_{1,1} \left(\frac{\vec{\tilde{E}}_N^-}{\vec{\tilde{E}}_N^+} \right) + \vec{\tilde{P}}_{1,2}}{\vec{\tilde{P}}_{2,1} \left(\frac{\vec{\tilde{E}}_N^-}{\vec{\tilde{E}}_N^+} \right) + \vec{\tilde{P}}_{2,2}}.\tag{2.4.11}$$

The above equation can be simplified by the substitute

$\frac{Z_s k_{z_N} \cos \theta_N - \omega \mu_N}{Z_s k_{z_N} \cos \theta_N + \omega \mu_N} e^{-i2z_N k_{z_N} \cos \theta_N}$ instead of $\left(\frac{\tilde{E}_N^-}{\tilde{E}_N^+}\right)$, leading to the following expression,

$$\tilde{R} = \frac{\tilde{E}_0^-}{\tilde{E}_0^+} = \frac{\tilde{P}_{1,1} \left(\frac{Z_s k_{z_N} \cos \theta_N - \omega \mu_N}{Z_s k_{z_N} \cos \theta_N + \omega \mu_N} e^{-i2z_N k_{z_N} \cos \theta_N} \right) + \tilde{P}_{1,2}}{\tilde{P}_{2,1} \left(\frac{Z_s k_{z_N} \cos \theta_N - \omega \mu_N}{Z_s k_{z_N} \cos \theta_N + \omega \mu_N} e^{-i2z_N k_{z_N} \cos \theta_N} \right) + \tilde{P}_{2,2}}. \quad 2.4.12$$

Note that z_N here is the left boundary of the N^{th} while Z_s is the surface impedance, sometimes known as substrate impedance, calculated at $z = z_N$.

2.5 Bi Characteristic Impedance Transmission Line and Conjugate

Characteristic Impedance Transmission Line

The equivalent model of the propagator dyadic model is the BCITL (Bi Characteristic Impedance Transmission Line) multi-section model or CCITL (Conjugate Characteristic Impedance Transmission Line) multi-section model. It is possible to model planar multilayer structures effectively both for lossless and lossy situations using a bi-characteristic-impedance transmission line (BCITL). Conversely, a conjugate characteristic impedance transmission line (CCITL) is a lossless model which cannot be used to model multi-section lossy transmission lines [114], [115], [116], [117], [118], [119]. For the sake of generality, we discuss the BCITL model as equivalent to the propagator matrix model. The bi-characteristic-impedance transmission line is considered to consist of N line sections. Each line section of length d_i is characterised by the (ABCD) parameters of a two-port network, also known as electrical chain line parameters or transmission line parameters [120], [121], [122], [123], [124], [125]. Note that (ABCD) parameters differ from the former ABCD matrix model discussed earlier. The propagation constant of the j^{th} line section in the multi-section model, β_j , is a counterpart of the wavenumber of the j^{th} layer in the propagator

matrix model, $\beta_j \equiv k_j$. The impedance of the j^{th} line section in the multi-section model is symbolized by Z_j and harmonizes with a geometrical intrinsic impedance of the j^{th} layer in the propagator matrix model, $Z_j \equiv \frac{\eta_j}{\cos \theta_j}$,

$$Z_j = \begin{cases} \eta_j \cos \theta_j, & \text{for TM polarization} \\ \eta_j \sec \theta_j, & \text{for TE polarization} \end{cases} \quad 2.5.1$$

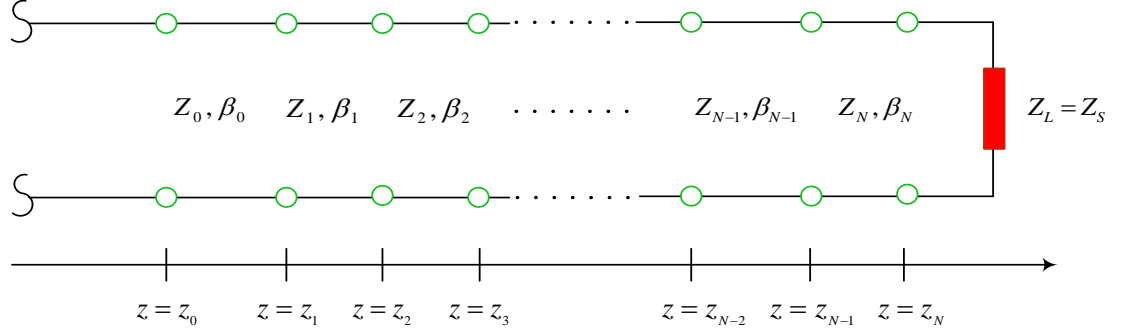


Figure 2.3 The model employed for a lossy transmission line with multiple sections, known as the bi-characteristic impedance transmission line (BCITL) model.

The total characteristic impedances, Z_{0b}^{\pm} , and the total propagation constant, β_b , in the BICTL model, can be calculated using the theory of a two-port network, (ABCD) parameters precisely, via the following, respectively.

$$Z_{0b}^{\pm} = \frac{\mp 2B}{(A - D) \mp i \sqrt{4 - (A + D)^2}}, \quad 2.5.2$$

$$\cos(\beta_b l_T) = \frac{A + D}{2}. \quad 2.5.3$$

The total reflection of the BICTL model, also known as input reflection, at $z = z_0$ is derived using the theory of a two-port network and mathematically computed using the input impedance, $Z_{in,b}$, by the following equation,

$$R_{in,b} = \frac{Z_{in,b} - Z_0}{Z_{in,b} + Z_0}, \quad 2.5.4$$

where the input impedance, $Z_{in,b}$, and the reflection at the load terminal, $R_{L,b}$, are defined as

$$Z_{\text{in},b} = Z_{0b}^+ Z_{0b}^- \left(\frac{1 + R_{L,b} e^{-i2\beta_b l_T}}{Z_{0b}^- - Z_{0b}^+ R_{L,b} e^{-i2\beta_b l_T}} \right), \quad 2.5.5$$

$$R_{L,b} = \frac{Z_s Z_{0b}^- - Z_{0b}^+ Z_{0b}^-}{Z_s Z_{0b}^+ + Z_{0b}^+ Z_{0b}^-}. \quad 2.5.6$$

where Z_s is the surface impedance, equal to the load impedance Z_L , calculated at $z = z_N$.

Ultimately, the section provided valuable insights into the latest trends and developments in various fields, shedding light on the fascinating world of multilayer thin films in materials science. These films, comprised of multiple layers of material, have a rich history and have been extensively studied since the early 20th century. Significant advancements in thin film deposition techniques, such as ion beam assisted deposition and molecular beam epitaxy in the 1980s, enabled the creation of precise and highly functional thin films with unique properties. Multilayer thin films are widely applied in electronics and optics due to their ability to tune the optical responses to electromagnetic waves.

Understanding and designing multilayer thin films involve theoretical modelling to predict their electrical and optical behaviours. Various approaches, including analytical models, numerical simulations, and first-principles calculations, play a crucial role in comprehending the underlying physical mechanisms and optimizing film properties. Important considerations include the film's conductivity, influenced by defects and charge accumulation, as well as its optical properties, affected by factors like refractive index, extinction coefficient, and layer thickness. Researchers employ mathematical methods such as the Transfer Matrix Method, polynomial approach, and ray transfer matrix to analyse how electromagnetic waves propagate through multilayer structures. Moreover, Maxwell's equations and finite difference time domain simulations serve as valuable tools for investigating the electrical and optical

characteristics of these films. The combination of experimental and theoretical approaches continues to drive advancements in thin film synthesis, characterization, and utilization.

CHAPTER 3

THEORY

3.1 Modelling of EM interactions with a multilayer structure using the polynomial method

The polynomial approach is one of the mathematical methods used for modelling the optical-electrical response of a multilayer thin film. The propagation matrix, $[\beta]_j$, mathematically represents the propagation of the electric field through a layer of j^{th} order. The interface matrix, $[A]_j$, mathematically represents the transition of the electric field from the layer of j^{th} order to the layer of $(j + 1)^{\text{th}}$ order at the interface region between them labelled as the j^{th} interface. The EM waves are assumed to propagate in the $+z$ direction and are defined as follows:

$$E^{\pm}(z_{j+1}) = [\beta]_j E^{\pm}(z_j + \delta_{z_j}), \quad 3.1.1$$

$$E^{\pm}(z_j + \delta_{z_j}) = [A]_j E^{\pm}(z_j), \quad 3.1.2$$

where z_j and z_{j+1} are the left boundaries and the right boundary of the j^{th} layer, while δ_{z_j} is the infinitesimal thickness of the interface at z_j .

The multiplication of the interface matrix with the propagation matrix alternatively will result in the mathematical representation of the overall structure. The polynomial approach excels in its detailed examination of the subtle effects caused by the extremely thin interface between layers in multilayer thin films, accurately representing this impact with clarity and precision. In contrast, other approaches may struggle to capture the intricacies of the thin interface between layers in multilayer thin films. They might oversimplify or overlook the subtle effects, leading to less accurate representations and potentially missing important details that could impact the overall understanding of the system. Our plan is to impose a lateral voltage on the multiple

thin film layers, leading to a change in the interface matrix. Therefore, the preferred technique for studying the optical and electrical behavior of the film is the polynomial method.

A general plane wave, which travels in a homogeneous, isotropic media, can be described by the following Maxwell's equations in the time domain of the SI system where \vec{E} is the electrical field, \vec{B} is the magnetic flux density, ϵ_0 , μ_0 , \vec{J}_{total} , and ρ_{total} are the permittivity of the vacuum, the permeability of the vacuum, current density, and charge density, respectively.

$$\vec{\nabla} \times \vec{E} + \frac{\partial \vec{B}}{\partial t} = 0, \quad 3.1.3$$

$$\vec{\nabla} \times \vec{B} - \epsilon_0 \mu_0 \frac{\partial \vec{E}}{\partial t} = \mu_0 \vec{J}_{\text{total}}, \quad 3.1.4$$

$$\vec{\nabla} \cdot \vec{E} = \frac{\rho_{\text{total}}}{\epsilon_0}, \quad 3.1.5$$

$$\vec{\nabla} \cdot \vec{B} = 0. \quad 3.1.6$$

Note that the tilde superscript denotes that the physical value is a complex number here and for the rest of the thesis.

Maxwell's equations can be rewritten, after some manipulations, into the following form, see Appendix B:

$$\vec{\nabla} \times \vec{E} + \mu_0 \tilde{\mu}_r \frac{\partial \vec{H}}{\partial t} = 0, \quad 3.1.7$$

$$\vec{\nabla} \times \vec{H} - \epsilon_0 \tilde{\epsilon}_r \frac{\partial \vec{E}}{\partial t} - \tilde{\sigma} \vec{E} = \vec{J}_{\text{ext}}, \quad 3.1.8$$

$$\vec{\nabla} \cdot \vec{E} = \frac{\rho_{\text{ext}}}{\epsilon_0 \tilde{\epsilon}_r}, \quad 3.1.9$$

$$\vec{\nabla} \cdot \vec{H} = 0. \quad 3.1.10$$